



LAWRENCE
LIVERMORE
NATIONAL
LABORATORY

Flow Around a Complex Building: Comparisons between Experiments and a Reynolds-Averaged Navier Stokes Approach

Ronald Calhoun, Frank Gouveia, Joseph Shinn, Stevens Chan, Dave Stevens, Robert Lee and John Leone

May 2004

Journal of Applied Meteorology, Vol. **43**, No. 5, pp. 696–710.

DISCLAIMER

This document was prepared as an account of work sponsored by an agency of the United States Government. Neither the United States Government nor the University of California nor any of their employees, makes any warranty, express or implied, or assumes any legal liability or responsibility for the accuracy, completeness, or usefulness of any information, apparatus, product, or process disclosed, or represents that its use would not infringe privately owned rights. Reference herein to any specific commercial product, process, or service by trade name, trademark, manufacturer, or otherwise, does not necessarily constitute or imply its endorsement, recommendation, or favoring by the United States Government or the University of California. The views and opinions of authors expressed herein do not necessarily state or reflect those of the United States Government or the University of California, and shall not be used for advertising or product endorsement purposes.

This is a preprint of a paper intended for publication in a journal or proceedings. Since changes may be made before publication, this preprint is made available with the understanding that it will not be cited or reproduced without the permission of the author.

This report has been reproduced
directly from the best available copy.

Available to DOE and DOE contractors from the
Office of Scientific and Technical Information
P.O. Box 62, Oak Ridge, TN 37831
Prices available from (423) 576-8401
<http://apollo.osti.gov/bridge/>

Available to the public from the
National Technical Information Service
U.S. Department of Commerce
5285 Port Royal Rd.,
Springfield, VA 22161
<http://www.ntis.gov/>

OR

Lawrence Livermore National Laboratory
Technical Information Department's Digital Library
<http://www.llnl.gov/tid/Library.html>

Flow around a Complex Building: Comparisons between Experiments and a Reynolds-Averaged Navier–Stokes Approach

RONALD CALHOUN, FRANK GOUVEIA, JOSEPH SHINN, STEVENS CHAN, DAVE STEVENS, ROBERT LEE, AND JOHN LEONE

Lawrence Livermore National Laboratory, Livermore, California

(Manuscript received 22 July 2002, in final form 11 September 2003)

ABSTRACT

An experiment investigating flow around a single complex building was performed in 2000. Sonic anemometers were placed around the building, and two-dimensional wind velocities were recorded. An energy-budget and wind-measuring station was located upstream to provide stability and inflow conditions. In general, the sonic anemometers were located in a horizontal plane around the building at a height of 2.6 m above the ground. However, at the upwind wind station, two levels of the wind were measured. The resulting database can be sampled to produce mean wind fields associated with specific wind directions such as 210°, 225°, and 240°. The data are available generally and should be useful for testing computational fluid dynamical models for flow around a building. An in-house Reynolds-averaged Navier–Stokes approach was used to compare with the mean wind fields for the predominant wind directions. The numerical model assumed neutral flow and included effects from a complex array of trees in the vicinity of the building. Two kinds of comparisons are presented: 1) direct experimental versus modeled vector comparisons and 2) a numerical metric approach that focuses on wind magnitude and direction errors. The numerical evaluation generally corroborates the vector-to-vector inspection, showing reasonable agreement for the mean wind fields around the building. However, regions with special challenges for the model were identified. In particular, recirculation regions were especially difficult for the model to capture correctly. In the 240° case, there is a tendency for the model to exaggerate the turning effect in the wind caused by the effect of the building. Two different kinds of simulations were performed: 1) predictive calculations with a reasonable but not high-fidelity representation of the building's architectural complexity and 2) postexperiment calculations in which a large number of architectural features were well represented. Although qualitative evidence from inspection of the angles of the vectors in key areas such as around the southeast corner of the building indicated an improvement from the higher-fidelity representation of the building, the general numerical evaluation indicated little difference in the quality of the two solutions.

1. Introduction

Experiments were performed to characterize the air-flow around a complex building. Several sets of experiments were performed that can be described in terms of “characterization of the wind field” and “releases of an inert gas.” In this paper, we report on the mean wind field and the modeling of the mean wind field with a Reynolds-averaged Navier–Stokes (RANS) approach.

Wind fields are important in both the wind engineering/building design literature and the literature on dispersion of atmospheric releases. Background reading on building aerodynamics can be found in a recent book by Lawson (2001). Becker et al. (2002) investigated experimentally the flow around blocks in a wind tunnel. Detailed quantitative information of turbulence in the

vicinity of the obstacle was obtained. Hort and Robbins (2002) performed laboratory experiments of dispersion and flow downwind of cylindrical buildings, with the presence of bunds, which significantly alter the flow patterns. Zhang et al. (1996) performed both numerical and physical modeling of stable atmospheric flow around a cubical building. They suggest that because the Froude number will rarely be less than 3 in the nighttime stable boundary layer, stratification will rarely be a significant factor influencing the flow structure in the near vicinity of a building. Smith et al. (2001) studied numerically the flow around a cubical building with radiatively induced thermal effects. They propose that because shading a building exerts local cooling, flows downstream from the building can be significantly affected. Higson et al. (1995) studied flow around somewhat more complicated model building shapes both in the free atmosphere and in a wind tunnel. They report that experiments in the wind tunnel tend to give higher estimates of mean concentrations as compared with the

Corresponding author address: Ronald J. Calhoun, Mechanical and Aerospace Engineering, Arizona State University, P.O. Box 876106, Tempe, AZ 85287-6106.
E-mail: ronald.calhoun@asu.edu

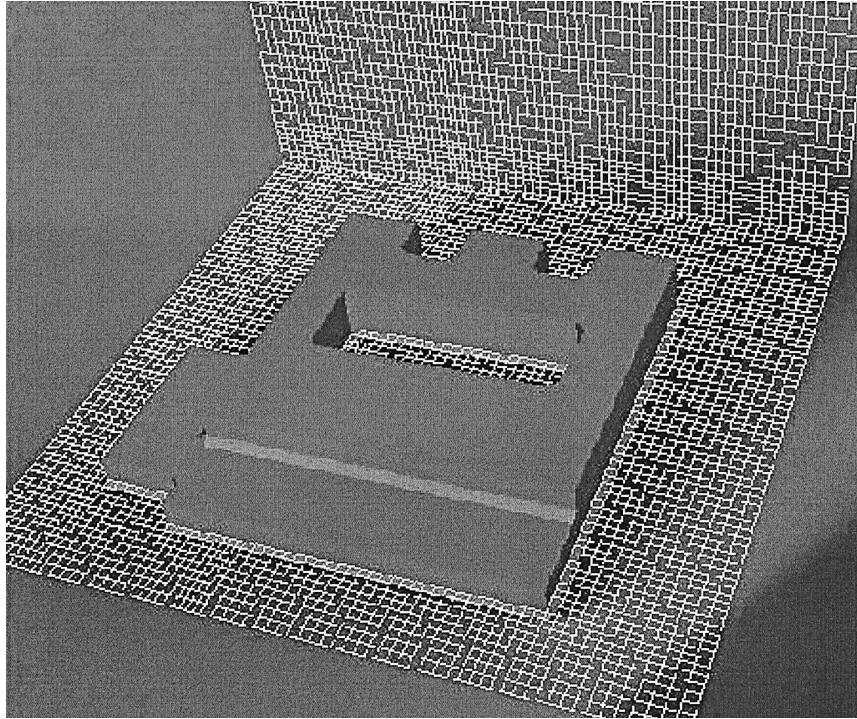


FIG. 1. The form of the computational model of the building—predictive simulations. The northerly direction is oriented toward the top. A subsection of the grid is shown. The whole grid extends beyond the domain pictured. Note that both of the architectural alcoves on the north side of the building, the building's two-level structure, and the inner courtyard are represented.

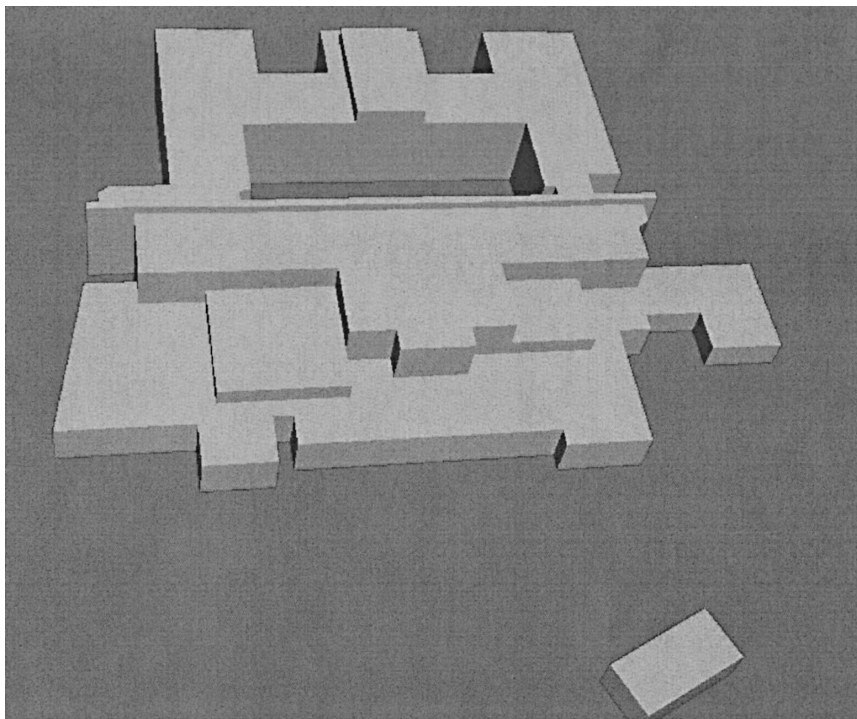


FIG. 2. Geometry for the building—postexperiment simulations. The northerly direction is oriented toward the top.

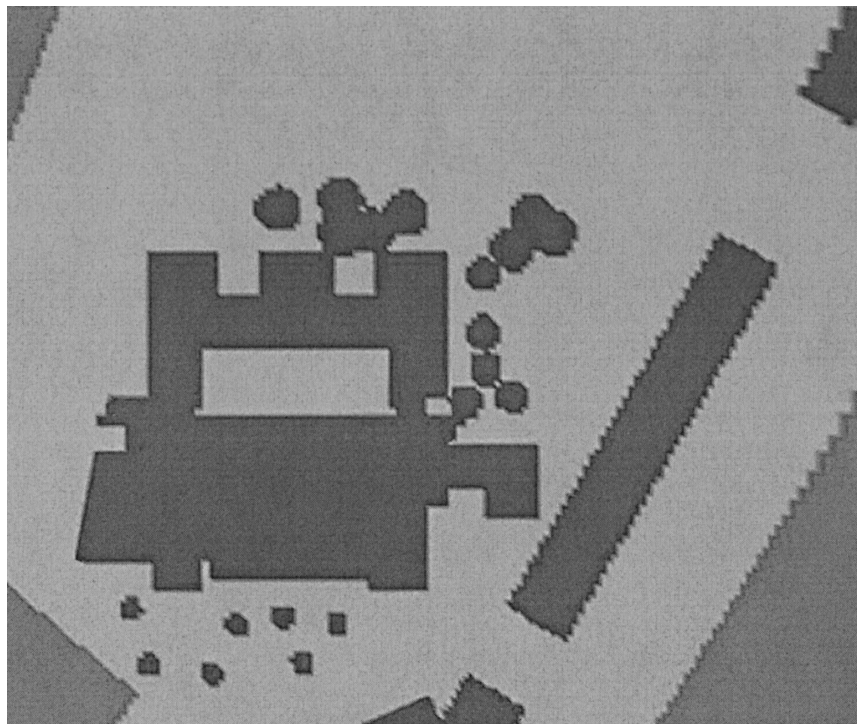


FIG. 3. The circular and the rectangular shaded regions are tree locations surrounding the building.

field data. This result presumably is due to the larger range of turbulent scales that are present in the atmosphere. Sagrado et al. (2002) numerically and experimentally studied dispersion in a street canyon. They found that increasing the height of the downstream building decreased concentrations in the street canyon.

Interest in flow around buildings can also be seen in recent conference proceedings. For example, Brown et al. (2000, 2001) and Calhoun et al. (2000) demonstrate modeling systems developed at U.S. Department of Energy national laboratories. Field studies using idealized layouts and representation of buildings have also been performed; see, for example, the Mock Urban-Setting Test field campaign using arrays of transportation containers to represent buildings (Zajic et al. 2002). Another important experiment that has direct relevance for flow around buildings is the Vertical Transport and Mixing/Urban Dispersion Experiment in Salt Lake City in autumn of 2000 (Allwine et al. 2002). The focus of this experiment was somewhat larger than a single building. The urban dispersion component of the experiment focused on dispersion from a gas release through multiple building blocks in the downtown area. A review of the literature shows an increasing interest in flow around buildings. However, whereas there has been a large amount of modeling and laboratory experiments performed, there have been relatively few full-scale wind and dispersion field experiments performed around single, complex buildings.

2. Plan and motivation

The first part of the experiment for flow around the building was concerned with measuring mean wind fields. As part of this study, the results of computer-simulated wind fields are compared with field measurements. This is the first stage of a larger effort to assess the ability of computational models to predict atmospheric dispersion scenarios around building complexes. This paper is focused on the simulation of the velocity field by a computational fluid dynamics (RANS) model. Two kinds of RANS simulations were performed: predictive and postexperiment. Predictive simulations were performed before the experiment primarily to provide initial guidance for the planning. By developing an approximate understanding of the major features of the flow field, the sensors could be more effectively deployed. The postexperiment runs were performed for two reasons:

- 1) The largest amount of experimental data was available for slightly different wind directions than the directions used in the initial calculations. The predictive runs simulated three wind directions— 200° , 225° , and 250° measured from true north. Although the winds did blow generally from the southwest (typical summer conditions for this site), the most appropriate data available were for 210° , 225° , and 240° .
- 2) The sensitivity of the predictions to various levels

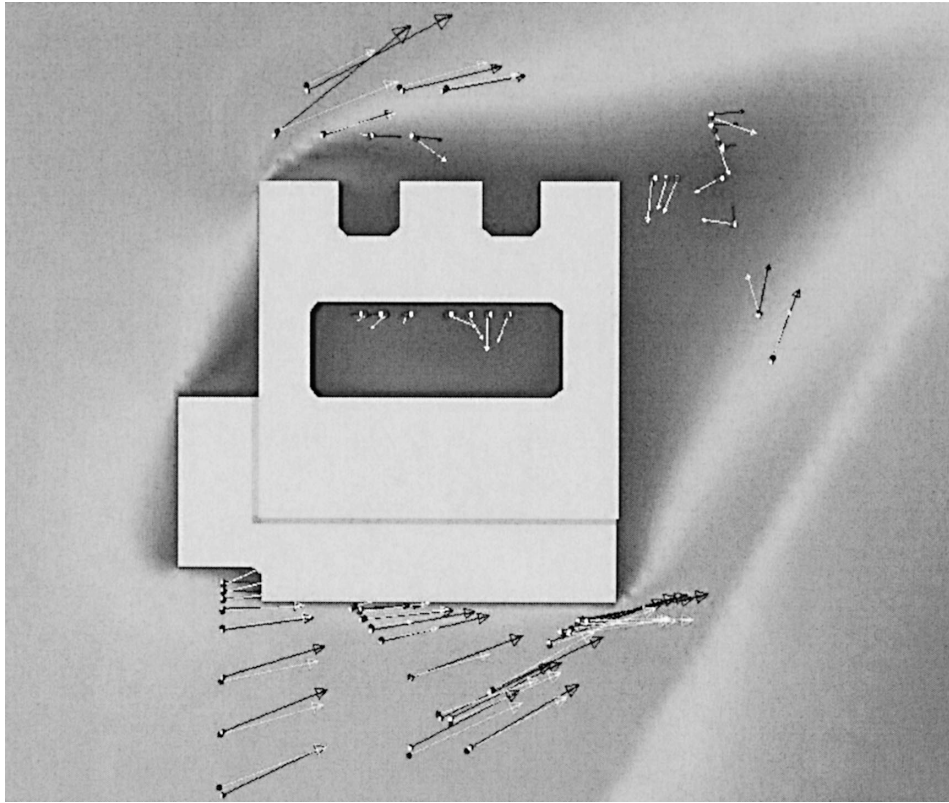


FIG. 4. Model and experimental vectors for predictive case— 225° winds. White vectors are experimental data, and black vectors are model data. Background shading represents modeled momentum, where low momentum is dark and high momentum is lighter.

of idealization that are by necessity a part of the modeling process should be explored. For example, what level of detail is required to model accurately the effect of the trees? How much architectural detail should be included in the model of the building? Figures 1 and 2 show the level of idealization of the building for the predictive and postexperiment cases.

The following sections will discuss the model setup and solution techniques, the experimental methods, and detailed comparisons of modeled versus experimental data.

3. Model setup and numerical methods

a. Neutral flow

The flow was assumed to be neutral, and no heat flux was imposed at the ground, a criterion that represents

cloudy, morning, or higher-wind conditions. As a consequence, only the experimental data that also represented neutral flow conditions were used in the following comparisons. The time of the year and conditions of the experiment were chosen so that neutral flow scenarios dominated for most of the duration of the experiment.

b. Canopy effects

Canopy effects (trees) were modeled with the addition of a drag term in the momentum equations. We follow, for example, Yamada (1982) and add the following term to the mean momentum equations:

$$\text{canopy_drag} = \eta C_d a(z) U |U|, \quad (1)$$

where η is the fraction covered by the canopy, C_d is the drag coefficient for the trees, $a(z)$ is the plant area density, and U is the x component of mean wind speed. An analogous term is used in the y direction.

In the predictive case, the canopy was modeled according to our conjecture that the major canopy effects were caused by a line of eucalyptus trees to the east of the building. To test this hypothesis, more-detailed canopy effects were included in the postexperiment runs. For example, in Fig. 3, the shaded circular areas sur-

TABLE 1. Predictive case— 225° .

Case	SAA	$m_{\text{dev}}/\text{ambient}$
Global	9	0.13
South	6	0.09
North	6	0.23
East	29	0.15

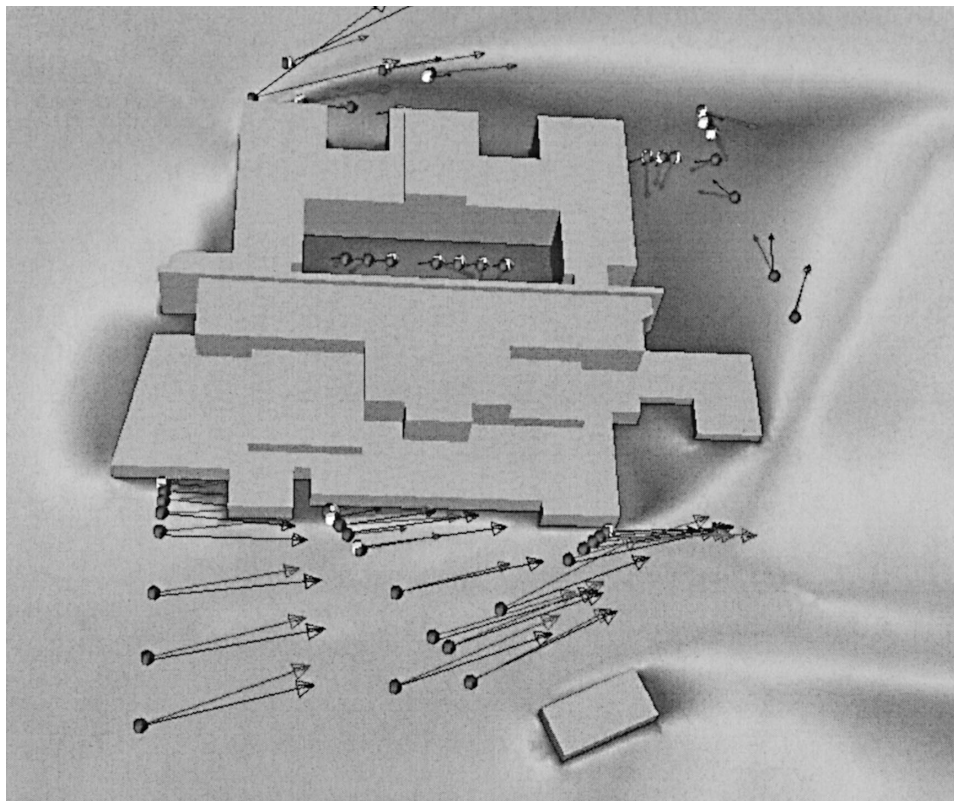


FIG. 5. Model and experimental vectors for postexperiment case—225° winds. Lighter-shaded vectors are experimental data, and black vectors are model data. Background shading represents modeled momentum, where low momentum is dark and high momentum is lighter.

rounding the building represent ornamental trees that surround the building and the shaded rectangular regions to the right of the building represent the row of eucalyptus trees, including major gaps in the row. In the vertical direction, the canopy is modeled as a two-layered structure in which a larger drag coefficient is assigned above the canopy base height and a lower drag is specified in the trunk area below the bulk of the limbs and leaves.

c. Wind directions

The wind directions used in the predictive study were 200°, 225°, 250° measured clockwise from true north (the prevailing winds at the building are from the southwest in the summer). The wind directions in the postexperiment cases were redone to match better the anal-

ysis of the measurements centered on the wind directions of 210°, 225°, and 240°.

d. Initialization, averaging, and duration of runs

To produce an initial field, a logarithmic profile modeled from data obtained at the upwind instrument station was assumed across the domain and a mass consistency requirement was enforced. The incoming wind profile was modeled as logarithmic with height with a maximum of about 3 m s^{-1} at the upwind height of 3 m. The averaging process in the equations of motions solved numerically is ensemble. The numerical procedure followed the traditional RANS approach. The duration of the run-time of a typical RANS simulation on local supercomputing platforms was less than 1 h.

e. Grid points and resolution

Approximately 1×10^6 grid points were utilized for the predictive run, and 2.5×10^6 were used for the postexperiment run. Grid stretching allowed the finest grid spacings near the building for the postexperiment case to be approximately 1 m. The computational domain spans $400 \text{ m} \times 400 \text{ m} \times 80 \text{ m}$, where the smaller dimension is in the vertical direction.

TABLE 2. Postexperiment case—225°.

Case	SAA	$m_{\text{dev}}/\text{ambient}$
Global	11	0.15
South	5	0.13
North	21	0.37
East	24	0.11

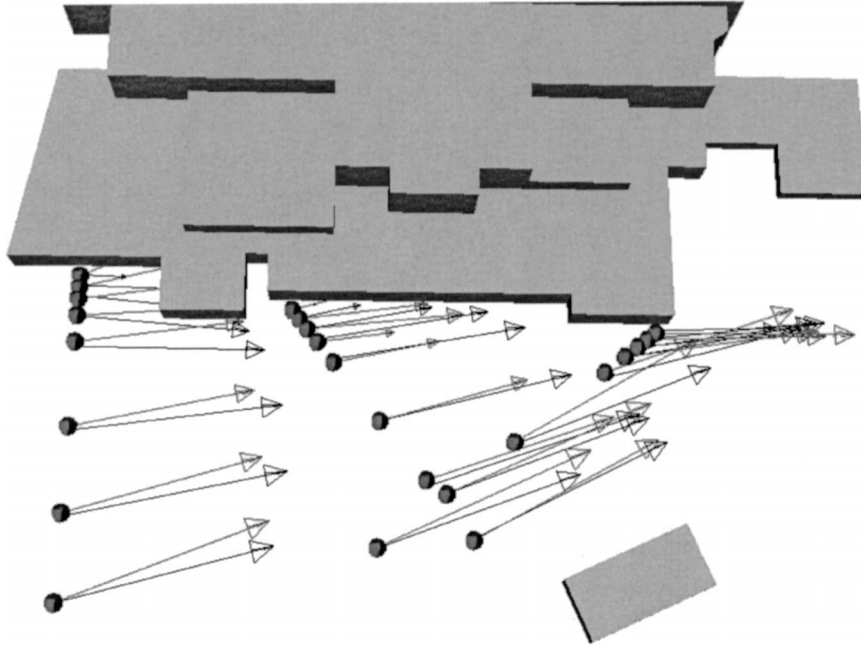


FIG. 6. The same as in Fig. 5 but for the south side only and no background shading.

f. Numerics and turbulence model

The computational fluid dynamics code utilizes a finite-element method (Chan 1987; Gresho and Chan 1998; Lee 1994; Chan and Lee 1999) and has been adapted for use on massively parallel computer plat-

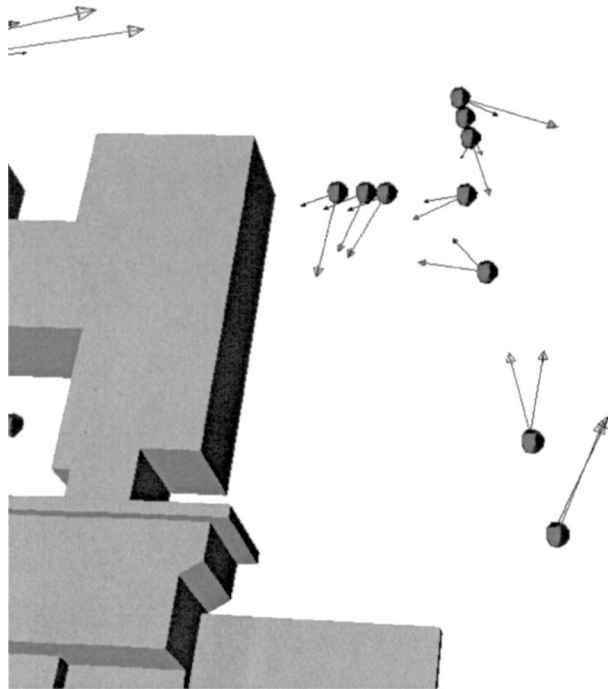


FIG. 7. The same as in Fig. 5 but for the east side only and no background shading.

forms (Stevens et al. 2000) through message-passing interface. The simulations performed here used 128 processors of the Advanced Simulation and Computing Program (ASCI) Blue-Pacific machine. A variety of different turbulent closures have been implemented and are available in the massively parallel code (see, e.g., Gresho and Chan 1998). The turbulence model used is the similarity- k turbulence model; that is, the turbulent fluxes are parameterized as proportional to gradients of mean variables. By changing an input option, our code may also be utilized in large-eddy simulation (LES) mode, whereby some of the turbulence is explicitly resolved and only the subgrid turbulence is modeled.

g. Why RANS?

The RANS solution procedure was evaluated for several reasons. This method is practical and should be tested for building scenarios because it is frequently used. Our experience is that the RANS approach uses about an order of magnitude less cpu time than the LES approach. In our view, each of these methods has an important place in the simulation of flows around buildings. RANS is adept at relatively cheaply calculating mean fields; LES is more expensive but allows information about the transient fields to be obtained. In short, if the level of information required involves the transient structure of the turbulent field, then LES would be the expected choice—because the large-scale motions are calculated rather than parameterized. However, RANS represents an effective compromise between cost and accuracy, a midpoint between extremely high resolution,

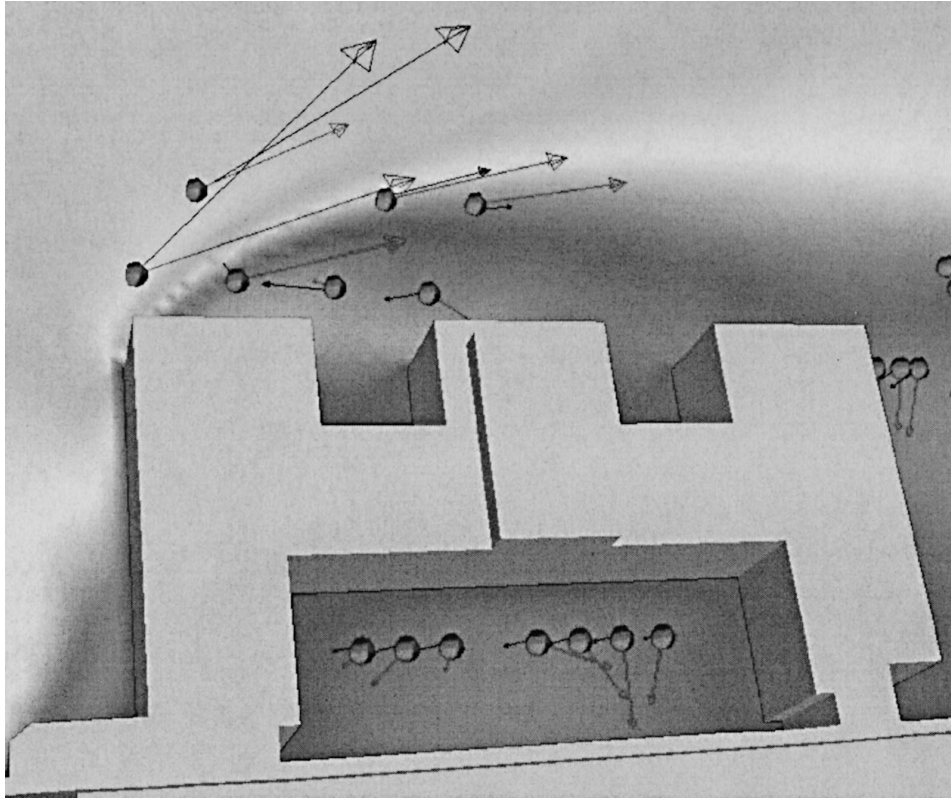


FIG. 8. The same as in Fig. 5 but for the north side only.

transient solutions and simpler but rapid response models such as Gaussian methods. For this reason, the RANS approach is evaluated for flow around a single complex building in the following.

4. Experiment and data collection

a. Goals and experimental strategies

The goal of the experiment was to provide airflow data around the exterior of the building that could be used to validate the computer models under development. One strategy was to make an estimate of the flow field using the predictive RANS calculations to determine placement locations for the wind sensors. Because a limited number of sonic anemometers were available, we employed a scheme that allowed us to, in effect, multiply the number of monitored locations. Measurements of velocity around the building were obtained by moving an array of eight sonic anemometers to a set of locations around the building—allowing the array to collect data for 5–7 days at each location for a total of 54 locations. Data from the resulting database can be chosen within a 15° window centered around a specified wind direction. The wind speeds are also normalized by dividing by the upwind wind speed observed at the same time. With this sorting and normalizing process, one mean field with the equivalent of 54 spatially distributed

sonic anemometers can be obtained for that wind direction. This scheme is repeated for several ranges of wind direction. The mean field comparisons presented later used a sampling of the database into 210° , 225° , and 240° wind directions. Although these values were representative of the major wind directions seen in the data, other ways of sampling the database would be possible.

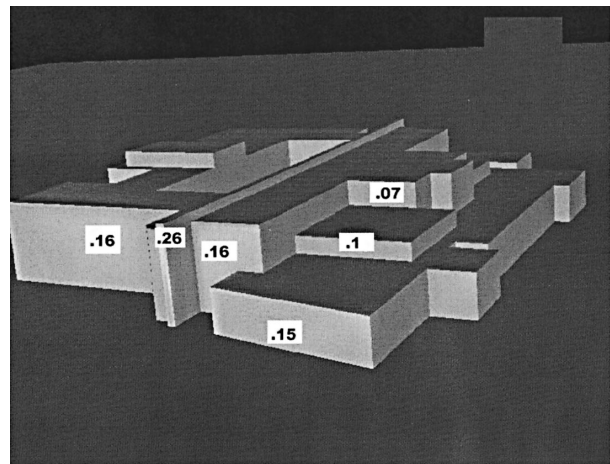


FIG. 9. Coefficient of pressure for postexperiment case— 225° winds.

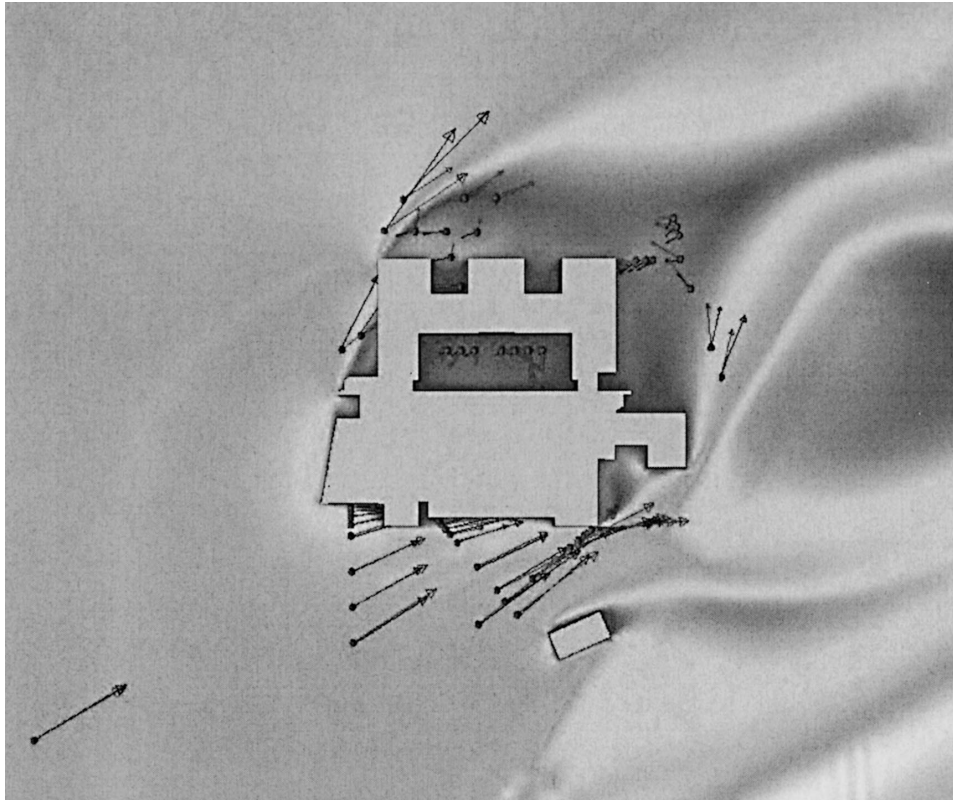


FIG. 10. Model and experimental vectors for postexperiment case— 210° winds. Lighter-shaded vectors are experimental data, and black vectors are model data. Background shading represents modeled momentum, where low momentum is dark and high momentum is lighter.

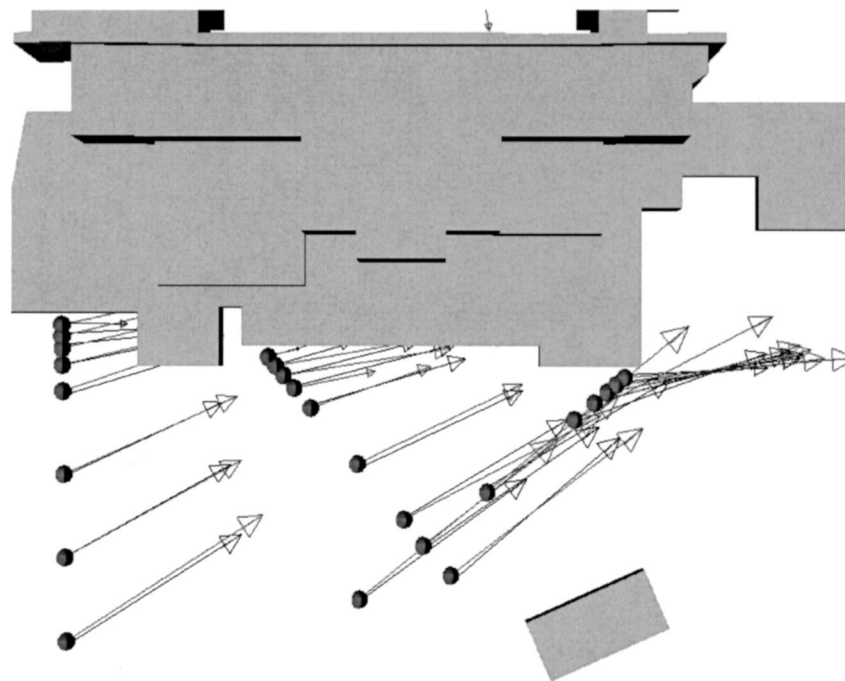


FIG. 11. The same as in Fig. 10 but for the south side only and no background shading.

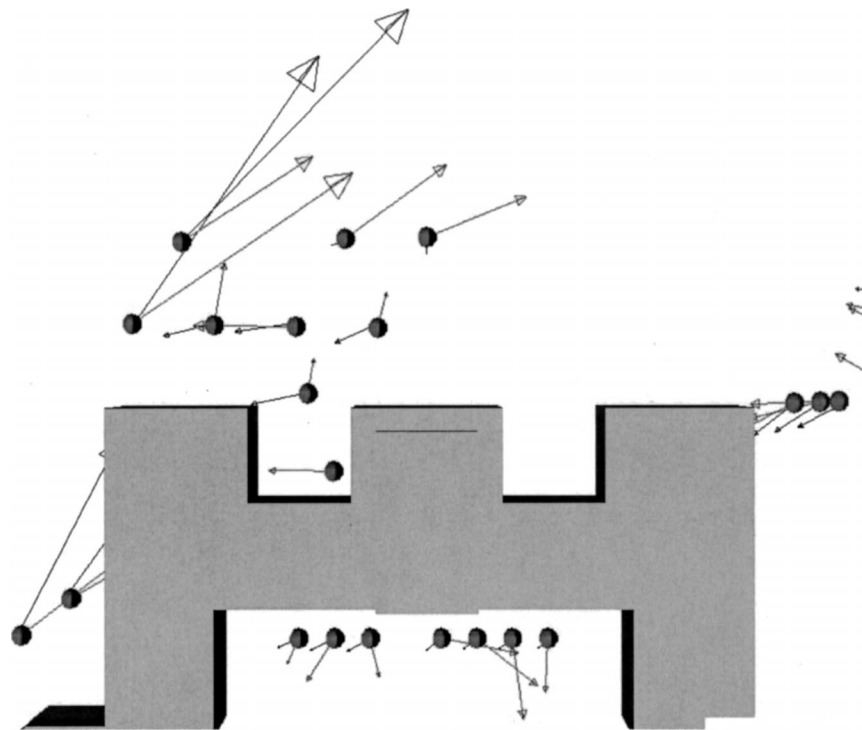


FIG. 12. The same as in Fig. 10 but for the north side only and no background shading.

The upwind reference station was an energy budget system that measured wind speed and direction as well as the sensible heat flux to the ground surface. Additional wind information was provided by an anemometer on top of the building and a permanent weather tower with wind measured at 10- and 40-m heights.

Because of normal variability in wind data, criteria were set up to determine which data would be rejected and which would be used for model validation. The long-term weather records from the permanent weather tower showed that at the 10-m height the median wind speed is 2.6 m s^{-1} and the 95th percentile is 6 m s^{-1} in annually compiled data (i.e., 5% of the wind speeds are greater than 6 m s^{-1}). During the summer months at the building site, the prevalent wind is from the southwest (SW), with recurrence frequencies of more than 60%. These recurrence frequencies reduce to about 20% by November. The first criterion was that the wind data should be retained when the wind direction was approximately from the SW; in practice all data were retained from the quadrant 195° – 285° . The second criterion was that with the above-mentioned definition of

“upwind,” the wind data should be retained when the wind speed exceeded 2 m s^{-1} and the atmospheric stability conditions were neutral at the energy budget reference station. The latter criteria provided assurance that the Monin–Obukhov length scale would be practically infinite for the inflow air upstream of the building.

It was decided to acquire the data in 1-s polls and to process them immediately into 10-min averages and standard deviations. The 10-min averages were to represent, in a time-averaged sense, meteorologically relevant mean variations of the winds at the measurement locations. The sonic anemometers (Vaisala, Inc., model 425) measured horizontal wind components only and were programmed to provide a pulse type of square-wave output sampled by the data acquisition system (Campbell Scientific, Inc., model CR-10). These dataloggers with two sonic anemometers each were normally able to operate in the averaging mode for 5–10 days without overwriting the memory buffers. In a special wind-variability study, the sonic anemometers were operated continuously at 1-s polls without preprocessing to average states. In these special cases, the dataloggers would overwrite the memory buffers in about 2 h. Quality assurance was provided by a quality-control procedure of inspection of sonic-anemometer performance in a slow-speed wind tunnel (1 – 2.5 m s^{-1}) and by the periodic quality-control normalization of placing all sonic anemometers at the same height and approximate location as the upwind energy budget station over 3–5 days (400–700 ten-minute periods). These quality-as-

TABLE 3. Postexperiment case— 210° .

Case	SAA	$m_{\text{dev}}/\text{ambient}$
Global	11	0.16
South	3	0.16
North	34	0.27
East	18	0.13

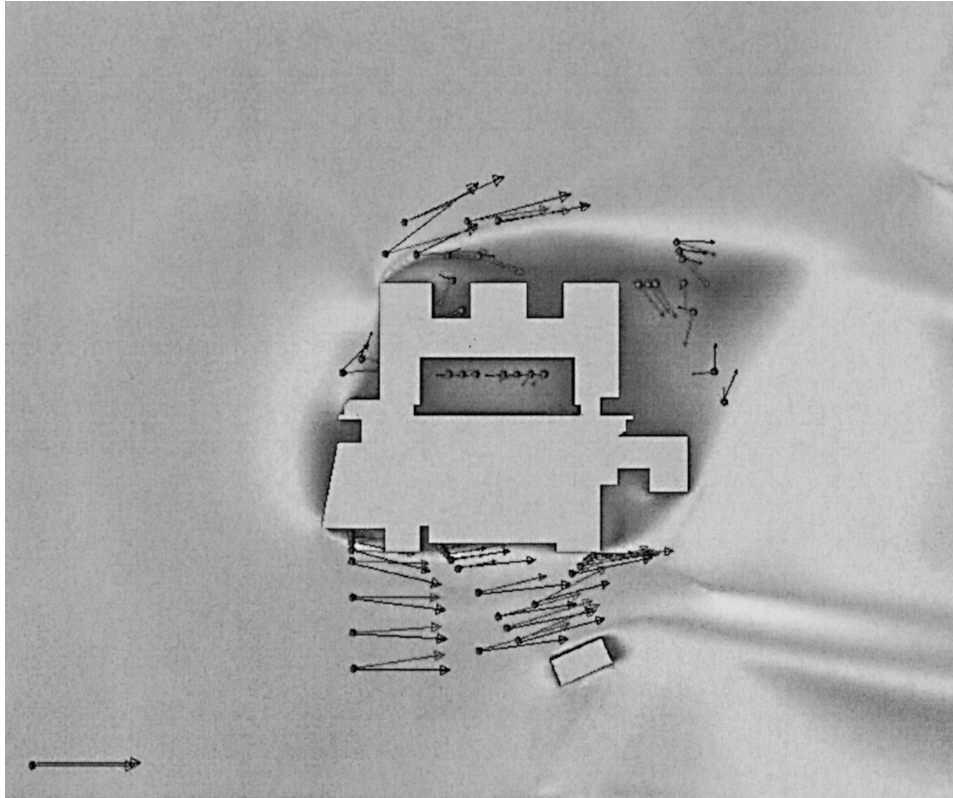


FIG. 13. Model and experimental vectors for postexperiment case— 240° winds. Lighter-shaded vectors are experimental data, and black vectors are model data. Background shading represents modeled momentum, where low momentum is dark and high momentum is lighter.

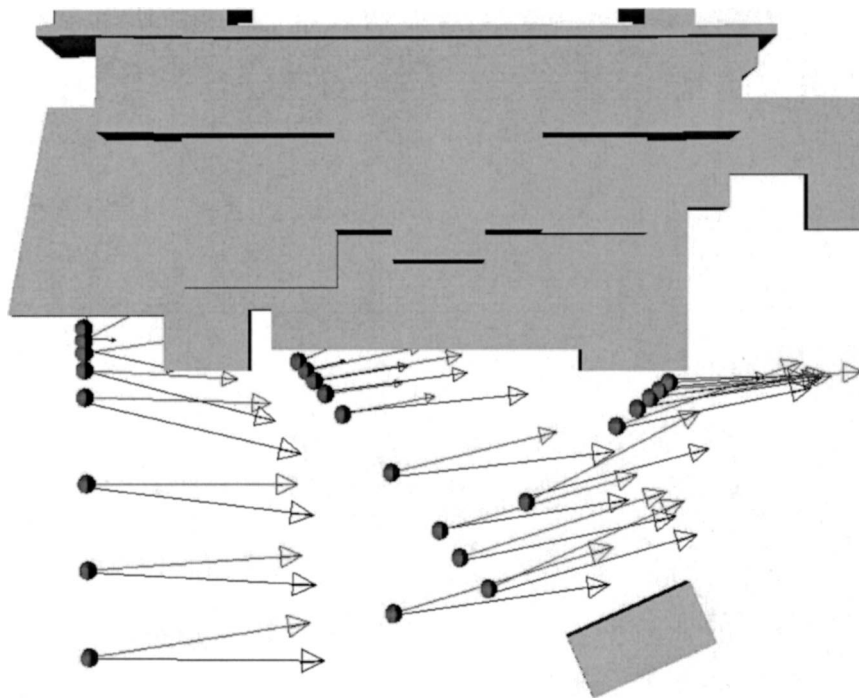


FIG. 14. The same as in Fig. 13 but for the south side only and no background shading.

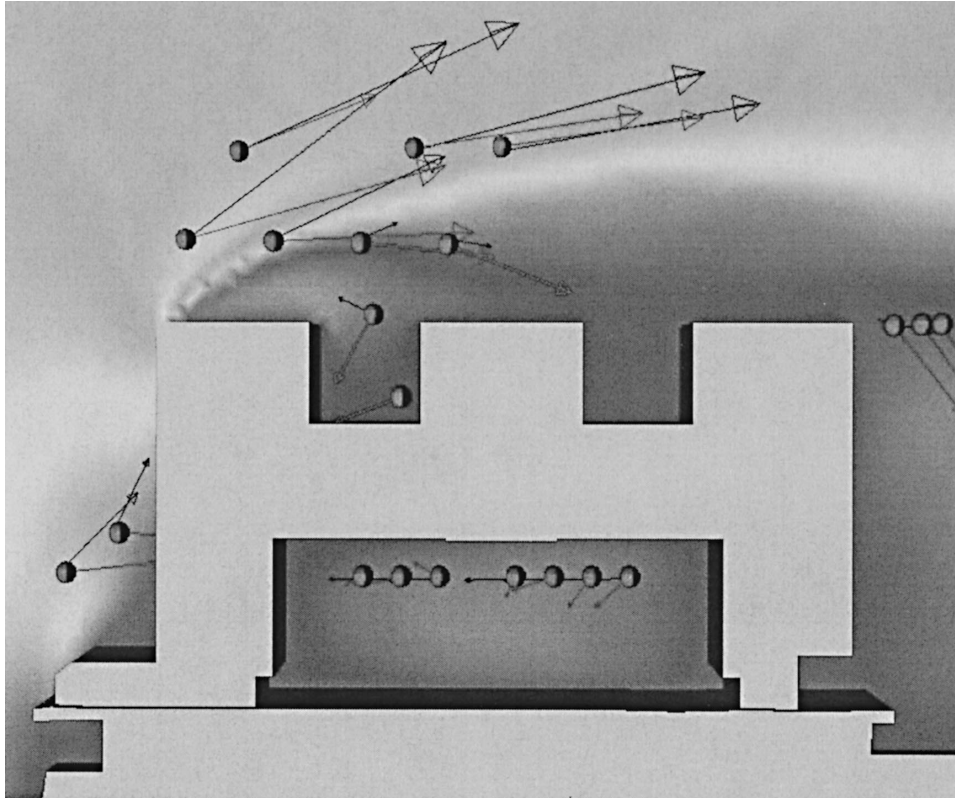


FIG. 15. The same as in Fig. 13 but for the north side only.

surance procedures give us confidence that the measurements were within 0.1 m s^{-1} when the speed was greater than 1 m s^{-1} . The only problems encountered were with one anemometer that proved to have a non-trivial calibration zero offset, two anemometers that required output span adjustments, and one failure caused by corrosion within the sonic-anemometer case. Because a spare sonic anemometer was retained, there was only a trivial amount of data lost.

b. Experimental dataset

Sonic anemometers were deployed eight at a time in arrays denoted as “stations.” Each station was allowed to acquire data for approximately 1 week. Reduction of the data in a spreadsheet allowed the data to be sorted according to the retention criteria, converted from conventional wind direction and speed to wind speed components, and then sorted by 10-min upwind wind direction. At this stage the component speed data were graphed according to upwind wind direction and were inspected. In this manner, wind speed components were seen to undergo a smooth transition in a continuous curve along the independent variable of upwind wind direction. This analysis showed that each 10-min period was representative and repeatable and was definitely not a random occurrence. Then data were combined into 5° bins to provide smoothing. These speed components

make up the dataset for 53 locations (one location was lost because of instrument failure). In addition, the same locations provided standard deviations of the wind direction for optional determination of turbulence intensity or approximate turbulent kinetic energy. A special study was undertaken to obtain a minimum of wind variability data for 6 of the 54 locations. In that study, six sonic anemometers were operated for 1 week with no 10-min summary, so that the memory buffers retained the 1-s data but filled up in about 2 h. Several 2-h periods that met the criteria were retained. From these periods, data collected for 1 h during the most persistent SW wind were retained as a benchmark dataset.

c. Strategy of sensor placement and divisions of data

The strategy of the sensor placement was to characterize as well as possible with a limited amount of sonic anemometers the flow field relatively near the building. The focus was on the deviation in the upwind flow caused by the building. We expected that each side of the building would have flow patterns unique to its location because of wind direction, blocking of the building, and canopy effects. Predictive RANS calculations supported this expectation. Second, we were well aware of the importance of capturing strong shears that occur near solid boundaries such as the building surface.

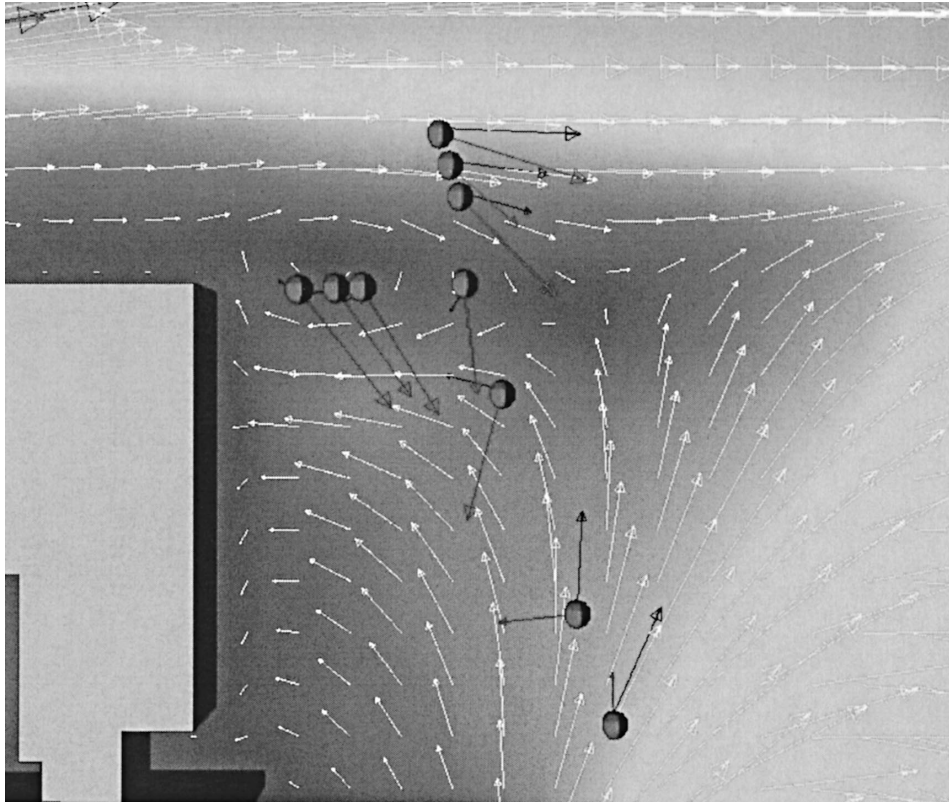


FIG. 16. The same as in Fig. 13 but for the east side only. The white vector field is the modeled wind not at measurement points (but at the same height).

When numerically simulating fluid-flow problems, our experience is that it is usually crucial to place a large number of grid resources near solid boundaries. Much of the turbulent kinetic energy, for example, is created in these areas. As a consequence, the sensor placement strategy reflected the importance of the regions near the building surface. The sonic anemometers were placed increasingly closer together (following a modified logarithmic distribution) in a line approaching the building for a region of interest.

The north and east sides of the building were expected to provide a chance to test models with recirculating flow conditions, and the south side represented angled flow toward a complex building surface—flowing, in addition, through a gap between a storage shed and the main building and also between a gap in the main tree line. The inner courtyard was also instrumented, because flow patterns over and into the courtyard determine whether it might be a safe haven or a potentially more

dangerous area in the advent of an atmospheric release in front of the building. These divisions, “north,” “south,” and “east” of the building help to group the data into categories that represent convenient ways to test computational approaches.

d. Data availability

The format of the data is in Microsoft, Inc., Excel spreadsheets and is generally available for researchers. At the time of writing, it could be obtained by contacting Frank Gouveia by e-mail at gouveia2@llnl.gov. By writing different conditional statements in Excel, the data could be sampled in ways other than we have described in this paper.

5. RANS model—Experimental comparisons

In the following, graphical and numerical comparisons between the experimental data and model results are given. The simplest and most illuminating method of comparison is to overlap experimental and model vectors at the sensor locations. It is more challenging to interpret numerical comparisons because one cannot see and easily evaluate the cause and importance of errors. For example, near a corner of the building there may be strong gradients and a recirculation zone where

TABLE 4. Postexperiment case—240°.

Case	SAA	$m_{\text{dev}}/\text{ambient}$
Global	12	0.15
South	7	0.15
North	11	0.24
East	51	0.18

strong positive velocities exist near small negative velocities. In addition to model errors, there may be small errors in the sensor locations that could potentially be important in regions of strong gradients. In these cases, it is important to see that the mean dynamics are well represented. Are the mean structures present with approximately the correct magnitudes and directions of rotation? We will provide this kind of analysis when needed to support numerical comparisons provided below.

a. Numerical measures of comparison

We compare magnitudes of the velocity vectors with mean absolute deviations. These deviations are defined as

$$m_{\text{dev}} = \frac{1}{N} \sum |U_{\text{mod}} - U_{\text{exp}}|. \quad (2)$$

In Eq. (2), N represents the number of sensor locations being compared and U represents the magnitudes of the experiment or the model depending on the subscript. This formula will be applied globally and by regions to the domain. The regions are defined as north, south, and east, where north is the top of the figures. There are not enough data to define a separate “west” region. Angles will be compared by using scaled average angle differences, defined as

$$\text{SAA} = \frac{\left(\sum |U_i| \phi_i \right)}{N \overline{|U_i|}}, \quad (3)$$

where ϕ_i is the angle between measured and modeled velocity vectors and N is the number of samples being averaged. The angle difference is scaled by the magnitude of the modeled velocity vector $|U_i|$ and then is normalized by the average of the magnitudes over the sample space. The purpose behind scaling the angles by the magnitudes is to weight the angles of the larger vectors more strongly. The justification for this approach is twofold: 1) the errors associated with the small vectors are relatively larger and 2), for transport purposes, angles associated with smaller vectors are less important than angles of larger vectors.

b. Predictive case—225° wind direction

Figure 4 shows sensor locations and the corresponding wind vectors for both the experimental data and the predictive model for 225° winds. Most of the sensor locations are on the south side of the building, and, in general, the agreement here is very good in terms of both velocity magnitude and direction. The major challenges remaining for this model in this area are to capture correctly the turning angle of the vectors as wind moves around the southeast corner of the building. The model predicted a stronger turning around the corner

than is observed in the experiment. We hypothesized that the over-turning of the modeled winds was a result of modeling the eucalyptus trees as a single, unbroken canopy region. In fact, there are large gaps in the tree line in several locations, one of them located near the southeast corner. Therefore, in the postexperiment runs, we test this hypothesis by including the gap in the trees. Notice that, on the north and east sides of the building, the mean dynamics are well represented. The direction of the recirculation on the east side is correct, and the vectors on the north side agree reasonably well. The model prediction for the courtyard was a helical pattern with flow exiting the northeast corner of the courtyard. A conclusive evaluation of the dynamics for the courtyard is not possible with the data available. It is clear, however, that the experimental vectors are larger in parts of the courtyard than the model anticipated. The discrepancy may in part be attributable to the ornamental vine-supporting structure in the center of the courtyard that was not included in the simulation.

Table 1 is distilled from a spreadsheet comparison of modeled and experimental data. The middle column describes how the angles compare and the last column compares magnitudes scaled by the magnitude of the ambient vector (the upstream wind vector). Notice that the angles (in degrees) compare well for the global, south, and north regions. The larger error in the angles on the east side is due to the difficulty of precisely modeling the position of features in the lee of the building. We elaborate on this discussion for the 240° case later. The errors in the magnitudes are less for the south side and are highest, relative to the ambient, near the north side.

c. Postexperiment case—225° wind direction

Notice in this case (Fig. 5; Table 2) that channeling between the gaps in the trees has developed and that this channeling has improved the angles on the south side of the building near the eastern corner. The recirculation on the east side displays the same counterclockwise rotating mean circulation that is found in the experimental data. The northern side shows a correct clockwise rotation, although experimental results show a recirculation tighter to the building than do the model results. Figures 6, 7, and 8 show magnified views of each of the regions. Lighter-shaded vectors are the experimental values; black vectors represent the model results. Surprisingly large values for the experimental results exist near the eastern side of the courtyard. These values are likely a result of additional ornamental structures in the courtyard. Higher-than-ambient velocities are present around the northwest corner of the building, and the model correctly predicts these values (although a larger value is predicted than is found in the experiment: 3.5 vs 3.1 m s⁻¹). A higher-than-ambient jet is not found near the southeast corner of the building (for either model or experiment at the sensor locations). Fig-

ure 9 shows the coefficient of pressure on the building surface. Notice that there are potentially significant pressure differences between various levels of the building. The intakes for this building are on the roof of the second level. A pressure difference of about 3 Pa exists across the building in the west–east direction. As in the predictive case, the south region shows good overall accuracy in both angle and magnitudes. As before, positioning of the north-side recirculation is somewhat more difficult to capture. Note that the overall level of accuracy is comparable to the predictive case at the current positions of the sensors. It is likely that improvements in the postexperiment model run may be found at other locations; for example, at higher locations or near the gaps of the trees.

d. Postexperiment case—210° wind direction

Figures 10, 11, and 12 compare vectors for the 210° case (Table 3). As in the previous case, the model agrees well with the experiment on the south side. The east-side recirculation is nearly as accurate, capturing reasonably well the correct mean circulation and approximate location. The challenge for this wind direction is on the north side. Both model and experiment find similar types of circulations, but the close proximity of very small recirculation values and nearly ambient velocities means that a small positioning error causes a large error in the vectors. The experiment does not find higher-than-ambient velocities near the northwest corner. The model does predict stronger-than-ambient velocities, but uncertainty in sensor location may be partially responsible. Near the southeast corner, the experiment does find wind speeds that are slightly higher than ambient. Peak model values at the sensor locations near the southeast corner are close, nearly reaching the ambient level.

e. Postexperiment case—240° wind direction

Figures 13, 14, 15, and 16 allow analysis of 240° winds (Table 4). In this case, the south side has generally good agreement, although there is a tendency for the model to exaggerate the turning effect of the building. For the north side, the model does better than in the previous case. Some discrepancies exist on the east side. A magnification of this area with surrounding model vectors in white (lighter shade is experiment and black vectors represent model results at sensor location as in previous cases) shows that there is a mean eddy with the same direction in both the experiment and the model. However, the limited number of velocity vectors from the experiment seems to suggest an eddy larger in size and shifted farther to the south by about one-fourth of the building's width. Therefore, even in this area where agreement is not on par with other regions, both the model and the experiment agree that there will be an area on the east side of the building that will experience west-flowing winds. The winds in the courtyard are

more nearly matched by the model vectors, perhaps because the ornamental features obstruct the flow along the line of sensors to a lesser degree. The two sensor locations along the west side of the building indicate that the model solution overextends the turning effect of the building (farther out into the flow field). Of interest, for this wind direction, the experiment does not show a higher-than-ambient jet near either the northwest or southeast corners of the building. Model results, however, predict a higher-than-ambient jet around the northwest corner.

6. Conclusions

A RANS computer model has been compared with experimental mean wind vectors for several wind directions. The model solution generally captures the mean dynamics of the flow field, and errors, when significant, can usually be at least partially attributed to features, such as recirculations vortices, that, although present, are shifted in space. However, the experiment has illuminated several areas in which the model solution might be improved. Especially challenging are regions of the flow where large velocities are near small recirculations; in these cases, uncertainty in the location of the sensors may be partially responsible for discrepancies. In addition, perturbations (caused by the building) in the angle of the vectors (relative to ambient winds) tend to attenuate more rapidly away from the building than the model predicts. The numerical metrics corroborate the impressions gained by inspection of the vector fields that most of the discrepancies between the modeled and experimental wind fields are small relative to the ambient winds. When considering the inherent level of uncertainty in atmospheric flows of this kind, the overall agreement between the modeled and experimental fields is good in most areas of the flow field, with the greatest challenges in the recirculations zones. The more detailed architectural version of the building and the surrounding trees did qualitatively appear to improve specific features of the flow field—most notably the improvement in the angle of the wind on the southeast corner of the building just before the air flows through the gap in the line of trees. However, according to the quantitative measures, the differences do not appear to be significant.

Acknowledgments. Special thanks are given to dedicated staff members Dean Hadley, Stan Martins, Jack Robson, Hal Goldwire, Roald Leif, Ron Pletcher, and Tom Schaffer. This work was performed under the auspices of the U.S. Department of Energy by the University of California, Lawrence Livermore National Laboratory.

REFERENCES

- Allwine, K. J., J. H. Shinn, G. E. Streit, K. L. Clawson, and M. Brown, 2002: Overview of URBAN 2000: A multiscale field

- study of dispersion through an urban environment. *Bull. Amer. Meteor. Soc.*, **83**, 521–536.
- Becker, S., H. Lienhart, and F. Durst, 2002: Flow around three-dimensional obstacles in boundary layers. *J. Wind Eng. Ind. Aerodyn.*, **90**, 265–279.
- Brown, M. J., M. Leach, J. Reisner, D. E. Stevens, S. Smith, S. Chin, S. T. Chan, and R. L. Lee, 2000: Numerical modeling from mesoscale to urban scale to building scale. Preprints, *Third Symp. on the Urban Environment*, Davis, CA, Amer. Meteor. Soc., 64–65.
- , and Coauthors, 2001: Multiscale modeling of air flow in Salt Lake City and the surrounding region. *Proc. ASCE Structures Congress*, Washington, DC, ASCE, 1–14.
- Calhoun, R., S. Chan, J. Leone, J. Shinn, and D. Stevens, 2000: Flow patterns around a complex building. Preprints, *11th Joint Conf. on the Applications of Air Pollution Meteorology with the Air and Waste Management Association*, Long Beach, CA, Amer. Meteor. Soc., 47–52.
- Chan, S. T., 1987: FEM3 model simulations of selected Thorney Island phase I trials. *J. Hazard. Mat.*, **16**, 267–292.
- , and R. L. Lee, 1999: A model for simulating airflow and pollutant dispersion around buildings. *Air Pollution VII*, C. A. Brebbia et al., Eds., WIT Press, 39–45.
- Gresho, P., and S. Chan, 1998: Projection 2 goes turbulent—and fully implicit. *J. Comput. Fluid Dyn.*, **9**, 249–272.
- Higson, H. L., R. F. Griffiths, C. D. Jones, and D. J. Hall, 1995: Flow and dispersion around an isolated building. *Atmos. Environ.*, **30**, 2859–2870.
- Hort, M., and A. Robbins, 2002: The dispersion of fugitive emissions from storage tanks. *J. Wind Eng. Ind. Aerodyn.*, **90**, 1321–1348.
- Lawson, T., 2001: *Building Aerodynamics*. Imperial College Press, 286 pp.
- Lee, R., 1994: Numerical modeling of 3-dimensional flow and pollutant dispersion around structures. *Environ. Software*, **9**, 175–187.
- Sagrado, A., J. Beeck, P. Rambaud, and D. Olivari, 2002: Numerical and experimental modelling of pollutant dispersion in a street canyon. *J. Wind Eng. Ind. Aerodyn.*, **90**, 321–339.
- Smith, W. S., J. M. Reisner, and C.-Y. J. Kao, 2001: Simulations of flow around a cubical building: Comparison with towing-tank data and assessment of radiatively induced thermal effects. *Atmos. Environ.*, **35**, 3811–3821.
- Stevens, D. E., J. B. Bell, A. S. Almgren, V. E. Beckner, and C. A. Rendleman, 2000: Small-scale processes and entrainment in a stratocumulus marine boundary layer. *J. Atmos. Sci.*, **57**, 567–581.
- Yamada, T., 1982: A numerical model study of turbulent airflow in and above a forest canopy. *J. Meteor. Soc. Japan*, **60**, 439–454.
- Zajic, D., H. J. S. Fernando, M. Brown, and M. Nelson, 2002: A field study of flow around a building. *Bull. Amer. Phys. Soc.*, **47**, 166.
- Zhang, Y. Q., S. P. Arya, and W. H. Snyder, 1996: A comparison of numerical and physical modeling of stable atmospheric flow and dispersion around a cubical building. *Atmos. Environ.*, **30**, 1327–1345.